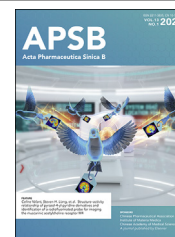




Chinese Pharmaceutical Association
Institute of Materia Medica, Chinese Academy of Medical Sciences

Acta Pharmaceutica Sinica B

www.elsevier.com/locate/apsb
www.sciencedirect.com



ORIGINAL ARTICLE

Actively separated microneedle patch for sustained-release of growth hormone to treat growth hormone deficiency



Li Yang^a, Qingyun Liu^a, Xinhui Wang^a, Nansha Gao^a, Xiuzhen Li^b,
Hongzhong Chen^a, Lin Mei^{a,c,*}, Xiaowei Zeng^{a,*}

^aInstitute of Pharmaceutics, School of Pharmaceutical Sciences (Shenzhen), Sun Yat-sen University, Shenzhen 518107, China

^bDepartment of Genetics and Endocrinology, Guangzhou Women and Children's Medical Center, Guangzhou 510623, China

^cTianjin Key Laboratory of Biomedical Materials, Key Laboratory of Biomaterials and Nanotechnology for Cancer Immunotherapy, Institute of Biomedical Engineering, Chinese Academy of Medical Sciences, Peking Union Medical College, Tianjin 300192, China

Received 26 January 2021; received in revised form 27 February 2022; accepted 18 March 2022

KEY WORDS

Microneedle;
Silk protein;
Self-administration;
Sustained-release;
Actively separated;
Growth hormone
deficiency;
Growth hormone;
Long-acting GH

Abstract Growth hormone deficiency (GHD) has become a serious healthcare burden, and presents a huge impact on the physical and mental health of patients. Here, we developed an actively separated microneedle patch (PAA/NaHCO₃-Silk MN) based on silk protein for sustained release of recombinant human growth hormone (rhGH). Silk protein, as a friendly carrier material for proteins, could be constructed in mild full-water conditions and ensure the activity of rhGH. After manually pressing PAA/NaHCO₃-Silk MN patch to skin for 1 min, active separation is achieved by absorbing the interstitial fluid (ISF) to trigger HCO₃⁻ in the active backing layer to produce carbon dioxide gas (CO₂). In rats, the MN patch could maintain the sustained release of rhGH for more than 7 days, and produce similar effects as daily subcutaneous (S.C.) injections of rhGH in promoting height and weight with well tolerated. Moreover, the PAA/NaHCO₃-Silk MN patch with the potential of painless self-administration, does not require cold chain transportation and storage possess great economic benefits. Overall, the PAA/NaHCO₃-Silk MN patch can significantly improve patient compliance and increase the availability of drugs, meet current unmet clinical needs, improve clinical treatment effects of GHD patients.

*Corresponding authors.

E-mail addresses: meilin@bme.pumc.edu.cn (Lin Mei), zengxw23@mail.sysu.edu.cn (Xiaowei Zeng).

Peer review under responsibility of Chinese Pharmaceutical Association and Institute of Materia Medica, Chinese Academy of Medical Sciences.

<https://doi.org/10.1016/j.apsb.2022.04.015>

2211-3835 © 2023 Chinese Pharmaceutical Association and Institute of Materia Medica, Chinese Academy of Medical Sciences. Production and hosting by Elsevier B.V. This is an open access article under the CC BY-NC-ND license (<http://creativecommons.org/licenses/by-nc-nd/4.0/>).

1. Introduction

Growth hormone deficiency (GHD) is a chronic disease with various causes¹. It leads to short stature (in children), abnormal metabolism, osteoporosis, etc., reduces the quality of life^{1–3}. In recent years, studies have shown that GHD can increase the risk of depression and anxiety in children and adolescents, seriously affect the physical and mental health of patients^{4,5}. The current treatment for GHD is an alternative therapy, namely daily subcutaneous (S.C.) injection of recombinant human growth hormone (rhGH), which has the same structure and pharmacological effects as endogenous GH. This method has been proven to be safe and effective after years of clinical practice⁶. However, GHD usually requires continuous treatment for many years, which brings thousands of S.C. injections to patients. Frequent dosing causes a heavy mental and economic burden on the patients and leads to poor compliance, thus obtaining suboptimal outcomes^{7–11}. According to a research survey in the United States, only 18.4% of medicaid patients and 32.3% of commercial patients persisted in the proportion of days covered was more than 80%, while more than 40% of patients stopped treatment before the age of 13¹². More importantly, the follow-up healthcare costs of untreated GHD patients are approximately twice than that of treated GHD patients. Therefore, GHD has become a significant healthcare burden, but many patients are still untreated or undertreated.

Developing a long-acting GH (LAGH) is an effective way to improve the compliance of GHD patients and the treatment effect¹³. To date, there are nearly 20 LAGHs reached various stages of development based on two basic approaches⁹. Increasing the half-life of GH through protein amplification technology is the most common method. However, this method will modify the molecular weight of GH, thereby changing the physical and chemical properties of GH, resulting in unpredictable clinical results. For example, an LAGH developed by Teva Pharmaceutical Industries, Ltd. that fused human serum albumin to the N-terminal gene of rhGH has produced neutralizing antibodies in the phase II of clinical trials for the treatment of GDH in children. Therefore, the development of the product was terminated¹⁴. Another method is to use reservoir or prodrug technology to achieve slowly release of unmodified GH. Considering that GH receptors are distributed throughout the body and have multiple functions, it would be safer and more effective to directly release unmodified GH which maintains the same tissue and organ distribution as endogenous GH. This method has produced two LAGHs that have been approved by the U.S. Food and Drug Administration (FDA)¹⁵. Unfortunately, despite LAGHs being available on the market, the available types and regions were extremely limited⁶. Cold chain transportation and storage were required to maintain active of LAGHs. Besides, professional medical personnel or medical device were needed to administration. These reasons lead to accessibility of LAGHs significantly reduce. Moreover, all marketed LAGHs require subcutaneous injection and inevitably cause injection pain, which is still not conducive to the management of GHD patients, especially for children. A survey from the Munich University Hospital showed that only 36% of adult GHD patients

are willing to receive LAGH treatment¹⁶. The management of GHD still faces great challenges.

Microneedle (MN) is a novel drug delivery system with minimally invasive manner^{17–19}. Most previous experience with MN has demonstrated self-management and painless administration^{20–22}. MN is a versatile platform mostly using solid MN or dissolving MN involved in the delivery of drugs or vaccines^{23–26}. Lee et al.²⁸ explored a water-soluble MN delivery rhGH. This type of MN still requires frequent administration, which cannot meet the current management of GHD. Based on the previous literature, most of LAGHs are made of biodegradable materials such as polylactic acid (PLA) and polylactic-co-glycolic acid (PLGA)^{27–29}. Organic solvents are unavoidable in the process of fabricating MN from these materials³⁰, which are not conducive to keeping the activity of proteins, such as rhGH. For example, Nutropin Depot is a LAGH built by PLGA which was approved by the FDA for treatment of GHD. rhGH was stabilized by forming an insoluble complex with zinc, which lead to a lengthy production process. This product was withdrawn from the market in 2004 due to high production costs and no market competitiveness³¹.

Silk fibroin, a protein extracted from silkworm, has good biocompatibility and biodegradability^{32,33}. Different from traditional sustained-release materials (such as PLGA), the processing of silk protein can be carried out under mild conditions of whole water³⁴. Two major structural models, termed silk I and silk II, have been reported for silk fibroin^{35,36}. Silk I refer to the complex helix-dominated structure, which is significantly different from the soluble random-coil dominated silk protein conformation of uncrystallized silk. Silk II is the insoluble antiparallel β -sheet crystal conformation³⁷. Therefore, the content of β -sheet in silk protein can be adjusted to achieve controlled release of therapeutics^{38,39}. To date, various methods have been used to induce β -sheet crystallization. For example, contact the silk protein with organic solvents such as methanol or ethanol^{40,41}, or expose silk protein to high humidity or high temperature conditions^{39,42}. In addition, studies have shown that biologically active substances can stably exist in dried silk membranes for a long period⁴². Researches on silk protein in sustained-release MN mainly focus on vaccines and contraception. One study reported a silk protein-based MN for long-acting contraception³⁸. These patches need to be worn throughout the drug release period, which is not conducive to the administration of GHD patients, especially for children, they are naturally active and have poor self-control. The development of an ideal LAGH MN requires the preparation process of MN is simple and mild, which is beneficial to directly encapsulate unmodified GH. The engineering of MNs that can be easily implanted into the skin and rapidly separated from the backing paper.

To address these challenges, we developed an active separation MN patch made from silk protein for the sustained release of rhGH. The active backing layer containing effervescent material NaHCO₃ was designed between the MNs and the backing paper. Thereby, MNs enabled to actively and quickly separate from the backing paper when applied to the skin. Subsequently, the backing was removed with no biohazardous sharps waste, which endows

good patient compliance through self-management. Detached MNs were embedded in the skin for slowly release of rhGH over 7 days. Silk protein was employed as rhGH-friendly carrier, got rid of the cold chain for transportation and storage of rhGH, greatly reduced costs and increased drug accessibility. We believe this MN patch can increase patients accessible to LAGH and improve clinical treatment effect.

2. Materials and methods

2.1. Materials

Silk protein was obtained from Simatech Biotechnology Co., Ltd. (Suzhou, China). Polyacrylic acid (PAA) ($M_w = 250$ kDa) was purchased from Sigma–Aldrich Biochemical Technology Co., Ltd. (Shanghai, China). Tetramethylrhodamine-6-isothiocyanate (TRITC), fluorescein5(6)-isothiocyanate (FITC, >96%) and sodium bicarbonate (NaHCO_3 , >99.5%) were purchased from Macklin Biochemical Technology Co., Ltd. (Shanghai, China). Recombinant human growth hormone (rhGH, >95%, $\text{C}_{990}\text{H}_{1528}\text{N}_{262}\text{O}_{300}\text{S}_7$, $M_w = 22$ kDa) was purchased from Nuptec Biotechnology Co., Ltd. (Hangzhou, China). PVP K90 was obtained from MBCHEM Co. (New Jersey, USA). Polydimethylsiloxane (PDMS, Sylgard 184 Silicone Elastomer Kit) was purchased from Dow Corning Co. (Michigan, USA). Human Growth Hormone ELISA kit and Mouse/Rat IGF-1 ELISA Kit were obtained from Multi Sciences Biotechnology Co., Ltd. (Hangzhou, China). Cell Counting Kit-8 (CCK-8) was purchased from Dojindo Molecular Technologies, Inc. (Kyushu, Japan).

2.2. Fabrication of MN patches

$\text{NaHCO}_3/\text{PAA}$ -Silk MN patch was prepared by centrifugal infusion PDMS mold method. PDMS mold was copied from the brass master mold contain a 12×12 array with a centre-to-centre interval of $750 \mu\text{m}$. The dimension of each needle was $300 \mu\text{m}$ in diameter and $800 \mu\text{m}$ in height. Briefly, silk protein was prepared into 100 mg/mL aqueous solution, then $200 \mu\text{L}$ solution was added to PDMS mold with pipette followed by centrifuged (Centrifuge 5910R, Eppendorf, Shanghai, China) for 10 min (4500 rpm , 4°C) to fill the caves. Residual silk protein solution was removed with a pipette. Subsequently, the mold was centrifuged at 25°C for 30 min to dry. Repeat the centrifugal filling and centrifugal drying operations to obtained silk needle tips with sufficient length. Then, PAA aqueous solution is added to the mold followed by centrifuged (Eppendorf) for 10 min (4500 rpm , 4°C). Similarly, remove the remaining liquid, centrifuged (Eppendorf) for 30 min to dry. Subsequently, suspend NaHCO_3 in the ethanol solution of PAA at a concentration of 1% (w/v), $\text{NaHCO}_3/\text{PAA}$ ethanol solution was fill the mold, centrifuged (Eppendorf) for 10 min (4500 rpm , 4°C), remove the excess solution, placed in a desiccator to dry overnight. The mold was taken out, fill it with PVP ethanol solution 20% (w/w), centrifuged (Eppendorf) for 10 min, put it in the desiccator again to dry overnight, untreated MN patch obtained.

For preparation of rhGH loaded $\text{NaHCO}_3/\text{PAA}$ -Silk MN, rhGH was dissolved in silk protein solution, and the subsequent preparation process is the same as $\text{NaHCO}_3/\text{PAA}$ -Silk MN.

To preparation of PAA-Silk MN, $\text{NaHCO}_3/\text{PAA}$ ethanol solution was replaced with PAA aqueous solution.

For preparation of PVP-Silk MN, PAA aqueous solution was replaced with PVP aqueous solution. PAA MN was fabricated by

direct centrifugation (Eppendorf) of PAA aqueous solution without silk protein.

2.3. Annealing of $\text{NaHCO}_3/\text{PAA}$ -Silk MN

After the silk protein solution was filled with the mold, the mold was taken out, placed in a constant temperature shaker at 37°C for 2 h (W-2 h) and 4 h (W-4 h), respectively, or put into a vacuum dryer with 100 mL methanol to annealing for 0.5 h (M-0.5 h). After the annealing was completed, mold was centrifuged for 30 min to dry. Annealing is required every time the silk protein solution is filled.

2.4. Mechanical strength test

The mechanical strength of $\text{NaHCO}_3/\text{PAA}$ -Silk MN, PAA-Silk MN and PAA MN was evaluated by a texture analyzer (TA-XT Plus, Stable Micro Systems, London, UK). Briefly, a single piece of MN patch was placed on the detection platform of the texture analyzer with the MNs facing upwards. The probe moved down according to the procedure until the MN was mechanically broken, the probe moved up immediately. The force change with the moving distance during the whole process was recorded.

2.5. Detachment test of the MN patches

To study the influence of the effervescent substance NaHCO_3 on the separation behavior of the MN patches *in vitro*, the MN patches were cut into single rows and fixed on the petri dish with double-sided tape. PBS solution was added to the petri dish to simulated the body fluid, the separation of different patches at different time points was observed and taken pictures using a fluorescence microscope (NIKON ECLIPSE Ti, Shanghai, China).

2.6. Skin insertion of the MN patches *ex vivo*

To better observe the penetrating effect of the MN patches on the isolated skin, TRITC-modified BSA was loaded into the MN patch as a model drug. Used thumb to press the patch into the isolated porcine skin. After 1 min, the backing paper was peeled off from the pig skin, the separation and penetration efficacy of the MN patch was observed with a stereo fluorescence microscope (SZ61-SET, Olympus, Japan).

In order to evaluate the drug delivery efficiency of the MN patch, the peeled backing and the incompletely penetrated MNs were carefully collected, and then released into the PBS solution for 20 days. The cumulative release of TRITC-BSA was determined by fluorescence quantitative method. The drug delivery efficiency in the MN patch was calculated by the amount of TRITC-BSA in the MN patch before implantation subtract the amount of TRITC-BSA in the backing paper and the MNs not inserted into the skin.

2.7. rhGH release from the MN patch *in vitro*

The TRITC-modified rhGH was loaded into the MN patch, release of TRITC-rhGH was quantified by fluorescence quantitative method. The MN patch obtained from different annealing methods was put into a centrifuge tube with 5 mL PBS solution as release medium incubated in a shaker water bath at 37°C and shaken at 100 rpm. All the released medium was collected and replaced equal volume of fresh release medium at different time points (2,

6, 12 h, and Days 1, 3, 5, 7, 10, 12, 14, 16). The content of TRITC-rhGH in the released medium was measured with a microplate reader (SpectraMax i3x, Molecular devices, Shanghai, China).

2.8. Fourier transform infrared (FTIR) spectroscopy

FTIR (Vertex 70 Hyperion 3000, Bruker, Billerica, USA) was used to characterize the secondary structure of silk protein⁴³. To explore the effects of different annealing conditions (W-2 h, W-4 h, M-0.5 h) on the secondary structure of silk protein, MNs treated with different annealing conditions were collected, and spectral scans were run from 1550 to 1750 cm^{-1} of each sample. The second-derivative and curve-fitting were used to analyse the results using the PeakFit v4.12 software (SeaSolve software Inc., Framingham, USA)⁴⁴. Exposed W-4 h MN to room temperature for one month, or immersed W-4 h MN to release condition for 16 days, the same method was used to investigate the secondary structure changes of silk protein before and after treatment.

2.9. The stability of rhGH in the MN patch

2.9.1. Circular dichroism (CD)

The classical CD was used to study the structural stability of rhGH during the preparation of MN patch or after exposure to room temperature for one month in the MN patch. Briefly, rhGH from freshly prepared MN or MN that has been placed in a desiccator for one month was extracted by release method. Subsequently, rhGH was concentrated by freeze-drying, the final concentration of rhGH was 10 $\mu\text{mol/L}$. Free rhGH was served as the control group, representing rhGH without any processing. The CD spectra of different treatment rhGH were acquired using a Chirascan spectropolarimeter (Chirascan, Applied Photophysics Ltd., UK). Spectra were recorded from 250 to 200 nm with bandwidth set at 1 nm. CD spectra were measured three times of each sample and the data of PBS buffer were subtracted as the blank.

2.9.2. Cell proliferation

To study the biological activity of rhGH during fabrication or placed in a desiccator for one month, Nb2-11 cell proliferation experiment was conducted⁴⁵. Briefly, cells were grown normally in 10% serum for three days, and then planted in a 96-well plate at a certain concentration, serum starved for one day. Subsequently, the rhGH to be tested in different concentrations was added. The concentration of rhGH from the MN was determined by the release profile of TRITC-rhGH *in vitro*. Considering that the release medium contained silk protein, the same concentration of silk protein was set as a control. After 2–3 days of culture, CCK8 was added with 2 h of incubation, the absorbance was measured at 450 nm with a microplate reader (Molecular devices) to calculate the cell proliferation.

2.10. In vivo pharmacokinetics of the $\text{NaHCO}_3/\text{PAA-silk MN}$

Male Sprague–Dawley (SD) rats (200 ± 10 g) were purchased from the Laboratory Animal Center of Sun Yat-sen University. All the protocols for experiments *in vivo* were approved by the Institutional Animal Care and Use Committee of Sun Yat-sen University. The SD rats were randomly divided into three groups, namely control group, subcutaneous (S.C.) injection group and $\text{NaHCO}_3/\text{PAA-Silk-rhGH MN}$ group. For S.C. injection group, 185 μg free rhGH per rat was injected, which is consistent

with the actual dose delivered by the $\text{NaHCO}_3/\text{PAA-Silk-rhGH MN}$. The dosage is calculated based on the drug delivery efficiency of MN *in vitro*. Before applying the MN patch, the hair of the mouse's back was shaved use a depilatory cream with gentle manner to avoid irritating the mouse's skin. After that, the $\text{NaHCO}_3/\text{PAA-Silk-rhGH MN}$ was pressed with thumb on the mouse's skin for 1 min, and carefully remove the backing paper.

Blood samples (~ 300 μL) were obtained from eye socket at 0, 0.25, 0.5, 1, 2, 6, 11 h and Days 1, 3, 7, 15, 25 after administration of MN patch. The blood samples were centrifuged at 4 °C to obtain plasma. The concentration of rhGH and IGF-1 in the plasma were measured with ELISA kit.

2.11. In vivo evaluation of the $\text{NaHCO}_3/\text{PAA-silk MN}$

2.11.1. GHD model mouse

To study the therapeutic effect of $\text{NaHCO}_3/\text{PAA-Silk-rhGH MN}$ *in vivo*, we constructed a rat model of hypophysectomy to simulate GHD⁴⁶. Male hypophysectomized rats were obtained from Cyagen Biosciences Inc. (Guangzhou, China). Rats were housed under a 12/12-h light/dark cycle and were provided with food and water ad libitum. Weigh the mice for three consecutive weeks, and the mice whose body weight does not fluctuate more than 10% are qualified model mice for further experiments. The weight of a qualified rat was 110–180 g.

2.11.2. Evaluate the therapeutic effect of $\text{NaHCO}_3/\text{PAA-Silk MN}$

The hypophysectomized mice that meet the requirements were randomly divided into three groups: one group was used as a negative control without any treatment; another group was received daily S.C. injection of rhGH for 21 days; the last group was $\text{NaHCO}_3/\text{PAA-Silk-rhGH MN}$ administration with once a week, for three consecutive weeks. At the same time, normal SD rats weighing 150–160 g were used as positive controls. To observe the effect of $\text{NaHCO}_3/\text{PAA-Silk-rhGH MN}$ on body weight, rats were weighed every three days during the treatment period. After the treatment, the body length of the mouse was measured. Subsequently, the tibia of rat was obtained, hematoxylin and eosin (H&E) staining of the tibia sections was performed to observe the changes in bone tissue. To evaluate the safety of the $\text{NaHCO}_3/\text{PAA-Silk-rhGH MN}$, the skin tissue of the administration site was collected for H&E staining observation after the treatment.

2.12. Degradation of $\text{NaHCO}_3/\text{PAA-Silk MN}$ *in vivo*

TRITC-modified silk protein was employed to fabricate $\text{NaHCO}_3/\text{PAA-Silk-rhGH MN}$ for visualization. The hair on the rat's abdomen was shaved and a MN patch was applied per rat. The fluorescence intensity at the administration site on Days 0, 1, 3, 7, 10, 14, and 21 after administration was measured by Spectrum living Image 4.0.

2.13. Statistical analysis

All results in this study expressed as mean \pm standard deviation (SD). Statistical analysis was performed by Student's *t*-test or an analysis of variance (ANOVA) test with Origin software (OriginLab, Northampton, MA), and *P* values < 0.05 were considered significant.

3. Results

3.1. Design and fabrication of active separation MN patch

To realize the active separation of the MN patch, we added the effervescent substance NaHCO_3 to the PAA separation layer formed active backing. PAA was chosen as the separation layer material because it is soluble in ethanol and water. PAA dissolved in ethanol could avoid reaction with NaHCO_3 suspended in ethanol during the fabrication of the MN patch. After the MN patch was applied to the skin, PAA absorbed the interstitial fluid of the skin (ISF) and produced H^+ , which reacted with NaHCO_3 to generate CO_2 and H_2O , realizing the active separation of the MN patch. The PAA/ NaHCO_3 -Silk MN patch was fabricated by multi-step centrifugation (Fig. 1B). In order to clearly distinguish the silk protein MNs, TRITC-modified silk was employed to fabricate PAA/ NaHCO_3 -Silk MN patch (TRITC-silk MNs were shown in red in Fig. 2A1). The engineered MNs were consistent in geometric dimensions with a base radius of 300 μm , a height of 800 μm , ~ 500 μm of silk protein MNs (Fig. 2A2). Particles were

observed in the active backing layer of PAA/ NaHCO_3 -Silk MN patch (Fig. 2A3) compared to PAA-silk MN patch (Supporting Information Fig. S1), which indicated effervescent substance NaHCO_3 was successfully introduced to the MN patch. The mechanical strength of MN patch prepared from PAA or silk protein was measured by texture analyzer. As shown in Fig. 1C, MNs made of PAA exhibited mechanical strength of approximately 78 N, while the mechanical strength of MNs was significantly improved by silk protein, its 181 N and 164 N of PAA-Silk MN patch and NaHCO_3 /PAA-Silk MN patch, respectively. The mechanical strength of the MN patch was slightly reduced by introducing NaHCO_3 to the active backing layer. All the patches still have enough strength to penetrate the skin.

3.2. Rapid separation test of active separation MN patch

To verify whether the MN patch could achieve rapid separation, the separation behavior of MN patches was investigated. TRITC-silk was used to prepare MNs for better visualization. MN patches were cut into single rows and fixed in a 10 cm dish. And then,

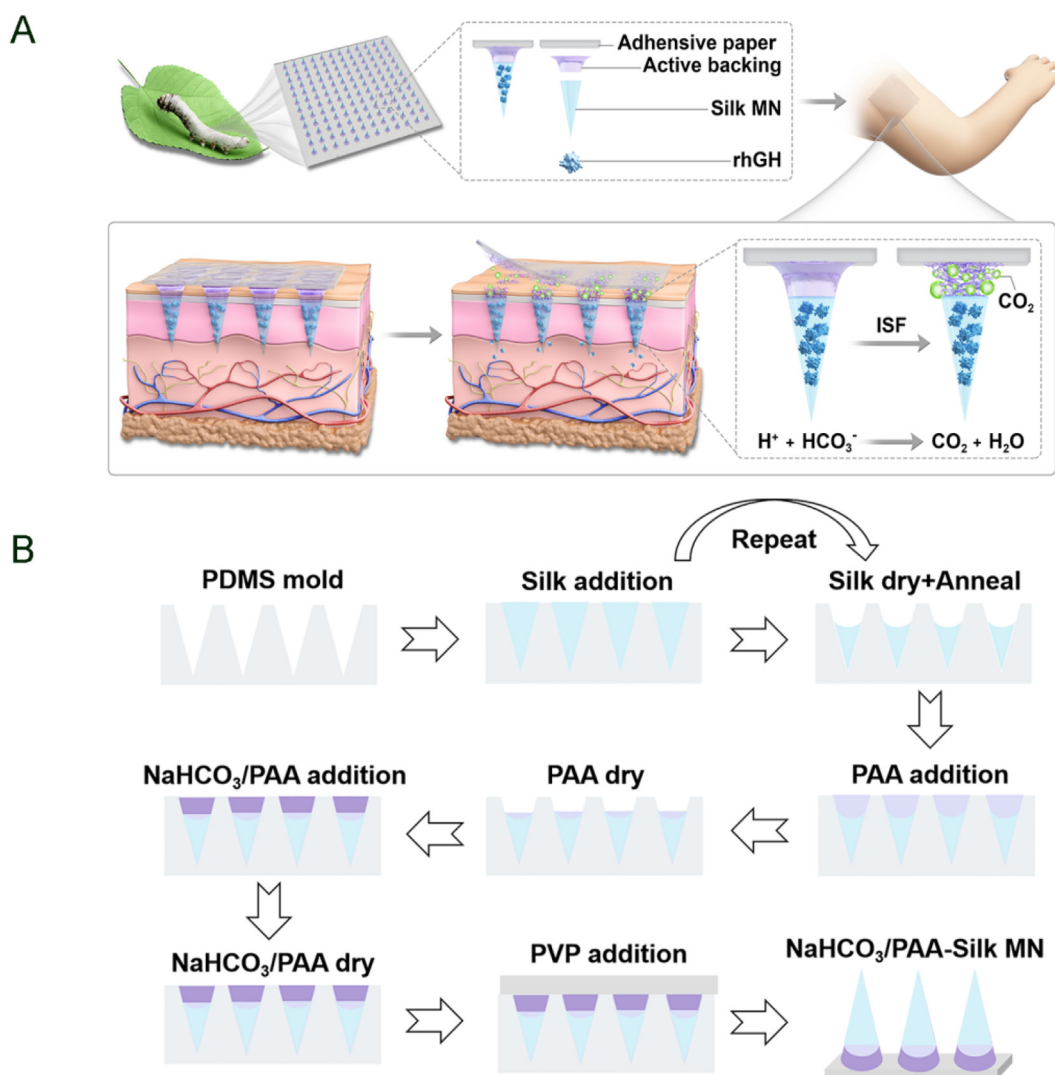


Figure 1 Design and fabrication of actively separated MN patch. (A) Schematic illustration of the design of an MN patch with active backing and the process of MN patch application to skin to achieve rapidly separated MNs from the backing paper by generating a lot of bubbles. (B) Schematic illustration of NaHCO_3 /PAA-Silk MN preparation process.

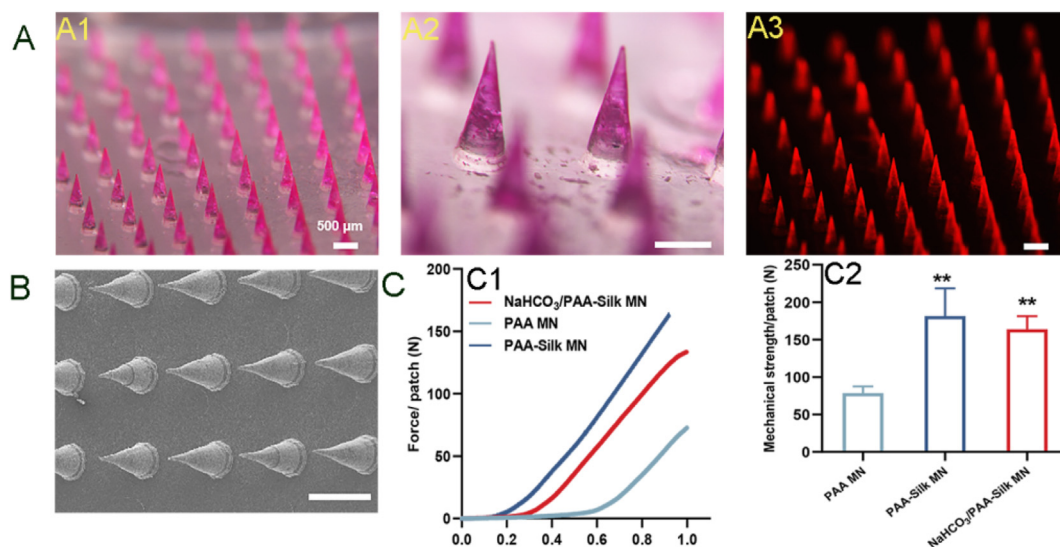


Figure 2 (A) Appearance of NaHCO₃/PAA-Silk MN patch. Bright-field photograph (A1-A2) and fluorescent photograph (A3) of NaHCO₃/PAA-Silk MN patch under a stereo fluorescence microscope. (B) NaHCO₃/PAA-Silk MN patch photographed by SEM. (C) Mechanical strength of MN patches. The force curve (C1) and mechanical strength (C2) of NaHCO₃/PAA-Silk MN patch, PAA MN patch and PAA-Silk MN patch. Data are mean ± SD, n = 3; **P < 0.01 vs. PAA MN patch. Scale bar = 500 μm.

phosphate-buffered saline (PBS) was added to the dish to simulate the separation that occurred after MN patches applied to the skin. Once PBS was added, the actively separated MN patch began to generate lots of bubbles to realize active separation (Fig. 3B). However, PAA-Silk MN patch without effervescent substance could only be separated by passively dissolving PAA (Fig. 3A). The separated MNs keep the structure intact (Fig. 3C and D). It only took 11.41 ± 0.43 s to complete the separation of MNs from the backing paper of active separation MN patch, compared to 80.81 ± 1.63 s for PAA-Silk MN patch and 71.53 ± 2.93 s for PVP-Silk MN patch (Supporting Information Fig. S5), which are

commonly used in nonactive MN patch formulation (Fig. 3E). These results demonstrated the active and rapid detachment of MNs from backing paper could realize *in vitro* by introducing NaHCO₃ into PAA separation layer.

3.3. Application of active separation MN patch to skin *ex vivo*

To observe the distribution of the drug and the separation layer in active separation MN patch, determine whether the MN patch could effectively deliver cargos. We loaded TRITC-BSA as a model drug into the MN patch, the fluorescent dye FITC was

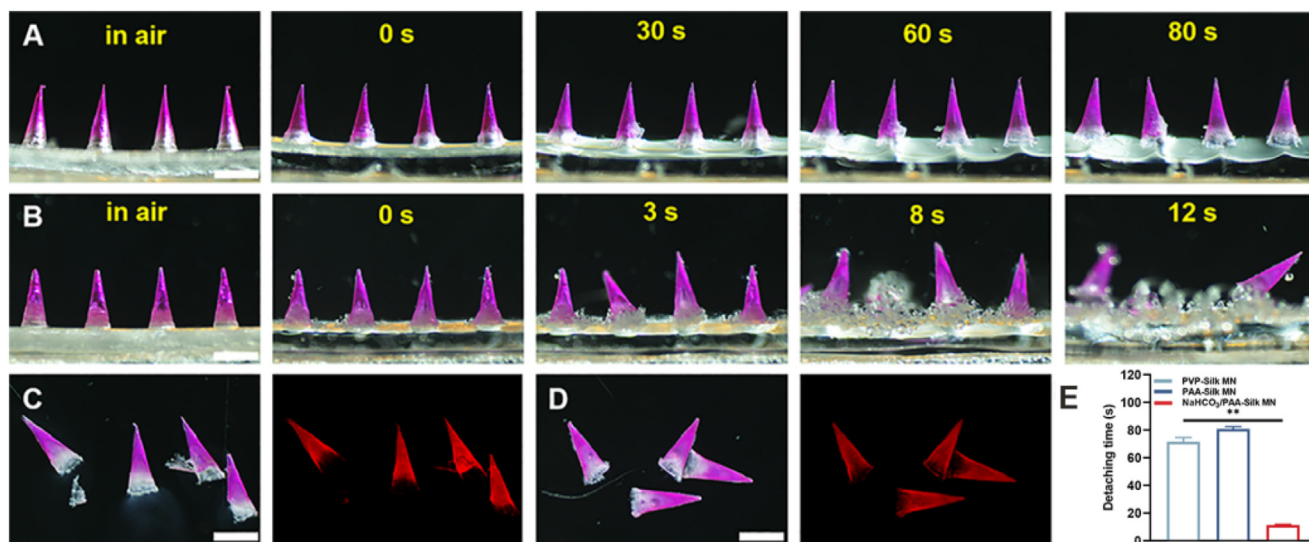


Figure 3 (A) *In vitro* separation behavior of PAA-Silk MN patch at different times in the PBS. (B) *In vitro* separation behavior of NaHCO₃/PAA-Silk MN patch at different times in the PBS. (C) Bright-field photograph and fluorescent photograph of MNs from PAA-Silk MN patch after separation. (D) Bright-field photograph and fluorescent photograph of MNs from NaHCO₃/PAA-Silk MN patch after separation. (E) Detaching time of MN patches contain PAA, PVP or NaHCO₃/PAA separation layer. Data are mean ± SD, n = 6; **P < 0.01 vs. NaHCO₃/PAA-Silk MN patch. Scale bar = 500 μm.

added to the PAA for preparing the separation layer. The active MN patch was cut into single rows and observed with CLSM. The loaded TRITC-BSA was mainly concentrated at the tip of the needles with a height of $\sim 500\ \mu\text{m}$ (Fig. 4A), which provided a guarantee for effective delivery of drugs by the MN patch. In order to more realistically simulate the separation of the MN patch after it was applied to the skin, explore the separation behavior of the MN patch. We tested MN patches using the porcine skin *ex vivo*. The tested patches were applied to porcine skin for 1 min, and then peeled off from the porcine skin. Microscopic observation of the skin at the administration site exhibited most of MNs from the actively separated MN patch could detach from the baking paper (Fig. 4C), while only a few MNs to complete the separation in PAA-Silk MN (Supporting Information Fig. S2). The detached MNs from the active separation MN patch were successfully implanted into the skin (Fig. 4B). The detachment efficiency of the active separation MN patch was over 95% compared to only 32% of the PAA-Silk MN patch. Similarly, the drug delivery efficiency of active separation MN patch was 4 times of PAA-Silk MN patch. The porcine skin penetration efficiency of the two MN patches was close to 100% (Fig. 4D). Together, these results implied rapid and efficient separation and high delivery efficiency could be achieved in *ex vivo* by using the active separation MN patch.

3.4. Long-acting behavior of rhGH from active separation MN patch *in vitro*

To explore the ability of the active separation MN patch to provide control release profiles of rhGH, we fabricated the MN patches with TRITC-rhGH and used fluorescence quantification to detect TRITC-rhGH released from MN patches dealt with different conditions. MN patches with different release behaviors were obtained through different annealing time or different annealing media. Without any annealing treatment on the MN patch, the release of TRITC-rhGH in 2 h was over 90%. Annealed with water for 2 h, The released of TRITC-rhGH from the MN patch was significantly reduced with around 50% in 2 h the release of TRITC-rhGH from the MN patch annealed in water for 4 h was further delayed with only $\sim 20\%$ of burst release in 2 h, and sustained release the remaining $\sim 80\%$ over 16 days. Conversely, the MN patch annealed with methanol for 30 min could obviously reduce the burst release in 2 h, with a similar sustained release profile with the patch annealed with water for 4 h (Fig. 5). Thus, varied release profiles could be obtained by controlling the annealing conditions of MN patches. Considering that methanol may be harmful to rhGH activity, we chose water-annealing for 4 h MN patch as a follow-up experimental investigation.

Generally, the mechanisms that control the drugs release from the sustained release formulations are dominated by diffusion, erosion, or combinations thereof. *In vitro* release curves of MN patches treated with different conditions were fitted with several classic release models to define the release mechanism of TRITC-rhGH from different MN patches (Supporting Information Table S1). As shown in Fig. 6B–D, all the patches fitted well to the Ritger–Peppas model. In the Ritger–Peppas model, if $n < 0.45$, molecules are mainly released by Fickian diffusion. This indicated that TRITC-rhGH released from all the patch was controlled by Fickian diffusion.

To further explore the mechanism of different annealing conditions affecting the release behavior of MN patches, we used fourier transform infrared (FTIR) to quantitatively analyze the

secondary structure of silk protein obtained under different conditions. Different processed silk proteins have different β -sheet content (Fig. 6A). With the extension of the annealing time, the β -sheet content was 34% for water-annealing for 2 h increased to 46% after water-annealing for 4 h, and the methanol-treated silk protein showed a β -sheet content up to 62%. The increase of β -sheet content indicated that the solubility of silk protein was reduced, and the resistance to drug release was increased, which was consistent with the results of *in vitro* release profiles.

It is worth noting that during the release period, the β -sheet content may continue to increase (β -sheet could induce by humidity environment, and this condition was provided during the release period). We compared the β -sheet content of water-annealing for 4 h MN patch and water-annealing for 4 h MN patch immersed in the release medium for 16 days. Interestingly, β -sheet content from 46% increased to 75% (Supporting Information Fig. S3A), and silk protein formed a stable water-insoluble structure, keeping the structure intact throughout the release period (Fig. S3B). These results further verified the release mechanism that the TRITC-rhGH was released through the Fickian diffusion, rather than the erosion of silk MNs. In summary, β -sheet content of silk protein was increased by annealing, the solubility of silk protein in water was reduced. Thus a relatively stable rigid structure of MNs was formed. The structure of MNs kept intact during the release period, and controlled drug release by Fickian diffusion *in vitro*.

Taking into account the characteristics of silk protein, structure changes may occur during storage, thereby affecting the release behavior of rhGH. We analyzed the secondary structure content of the MN patch (treated with water for 4 h) after being placed at desiccator (room temperature) for one month to verify the stability of the MN patch during storage (Fig. S3C). After being exposed to room temperature for one month, the secondary structure content of the silk protein in the MN patch, especially the β -sheet content, which significantly influences the release behavior of rhGH, showed no obvious change. Therefore, it was speculated that the secondary structure of the MN patch can be maintained at room temperature for at least one month without affecting the release behavior of rhGH.

3.5. Stability and activity of rhGH in active separation MN patch

Based on previous literature studies, silk protein can maintain the activity of proteins at room temperature for more than one month. We expect that the MN patch prepared from silk protein can realize the room temperature transportation and storage to reduce the cost. To verify whether the MN patch could ensure the activity of rhGH at room temperature, the MN patch was put in a desiccator at room temperature for one month, and then the rhGH was extracted to test if the structure and function were preserved.

Circular dichroism spectroscopy (CD) was employed to examine the structure stability of rhGH. There was no significant change to rhGH secondary structure after process or exposure to room temperature for one month (Fig. 7A). Subsequently, activity of rhGH was assessed by an established cell proliferation assay. Nb2-11 cells proliferate under the stimulation of GH. As shown in Fig. 7B, exposure of Nb2 cells to unencapsulated rhGH or extracted rhGH from the MN patches, all groups exhibited stimulation of cell proliferation with a function of rhGH concentration. These results displayed that the stability of the structure and activity of rhGH were preserved not only during the processing of

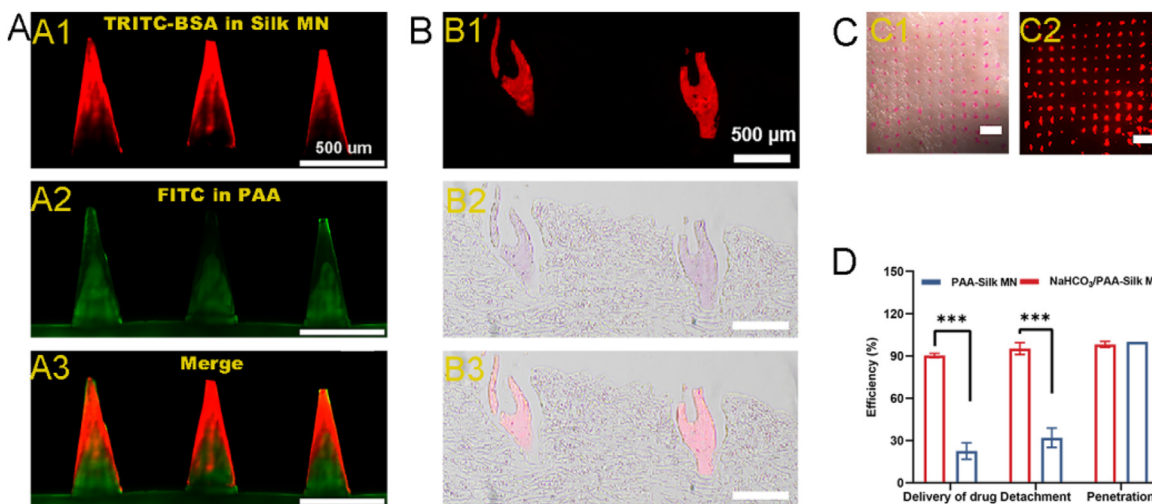


Figure 4 (A) Distribution of drugs in NaHCO₃/PAA-Silk MN patch. (A1) CLSM image of TRITC-BSA in NaHCO₃/PAA-Silk MN patch. (A2) CLSM image of FITC PAA in NaHCO₃/PAA-Silk MN patch. (A3) Merge image of A1 and A2. Scale bar = 500 μm. (B) Histological images of microneedles embedded in porcine skin *ex vivo*. Bright-field (B1) and fluorescence microscopy images (B2) of representative histological sections of porcine skin after NaHCO₃/PAA-Silk MN patch insertion, (B3) Merge image of B1 and B2. (C) Bright-field (C1) and fluorescence microscopy images (C2) of porcine skin *ex vivo* after NaHCO₃/PAA-Silk MN patch insertion. (D) Quantification of the efficiency of penetration, detachment and delivery of TRITC-rhGH from MN patches with or without active backing. Data are mean ± SD, n = 6; ***P < 0.001.

the MN patch, but also after the MN patch was placed at room temperature for one month.

3.6. rhGH pharmacokinetics and activity from active separation MN patch *in vivo*

To explore the pharmacokinetics of rhGH after release from the active separation MN patch *in vivo*, SD rats were each applied an MN patch, which was administrated to skin for 1 min (Supporting Information Fig. S6B). rhGH concentration in rat plasma reached a peak concentration of 57.70 ± 6.92 ng/mL at a time of 6 h after MN patch

application. Subsequently, the concentration of rhGH in the plasma gradually decreased and remained higher rhGH concentration than that in the control group for more than 7 days. However, the S.C. injection group obtained a peak concentration of 70.35 ± 8.87 ng/mL at 0.5 h, dropped the concentration of rhGH to the control group level after 11 h (Fig. 8A). The area of under the plasma concentration time curve (AUC) for rhGH delivery from the active separation MN patch was 148.90 ± 19.23 ng·day/mL compared to S.C. injection which was 6.58 ± 0.88 ng·day/mL (Table 1). These results indicated that the MN patch could successfully controlled release of rhGH *in vivo* for more than 7 days.

IGF-1 is an endocrine hormone mainly produced by the liver. It is an active protein polypeptide substance necessary for the physiological effects of GH, which induces production of IGF-1. Therefore, IGF-1 can be used as a biomarker of hGH activity. We conducted the concentration of IGF-1 in rat plasma to verify the biological activity of rhGH from the MN patch. The IGF-1 levels were significantly elevated both in S.C. injection group and the MN patch group compared to control group. The MN patch could keep a high level of IGF-1 over 15 days (Fig. 8B). In general, these results prove the key functions of the active separation MN patch: 1) achieving sustained release of rhGH over 7 days, 2) keeping the biological activity of rhGH.

3.7. *In vivo* evaluation of the active separation MN patch

To further explore the therapeutic effects of the MN patch on GHD, we conducted experiments using hypophysectomized mice as a model of GHD. In this study, each rat was applied one patch every week for three consecutive weeks. Rats were received daily S.C. injection of rhGH, continuous injection for 21 days as a comparison. Simultaneously, model rats without any treatment were used as a negative control group, and normal rats without any treatment were used as a positive control group. The results displayed in Fig. 9A shown that the length and weight of the rhGH-treated groups improved compared with the untreated negative

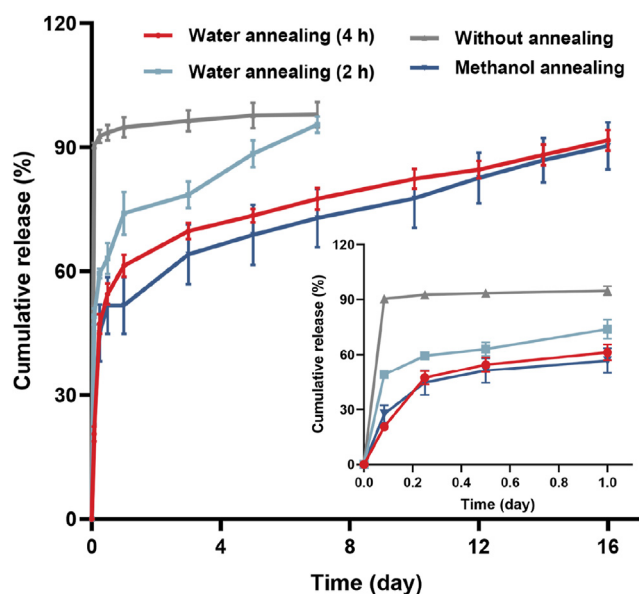


Figure 5 *In vitro* release profiles of MN patches with different annealing conditions. Data are mean ± SD, n = 3.

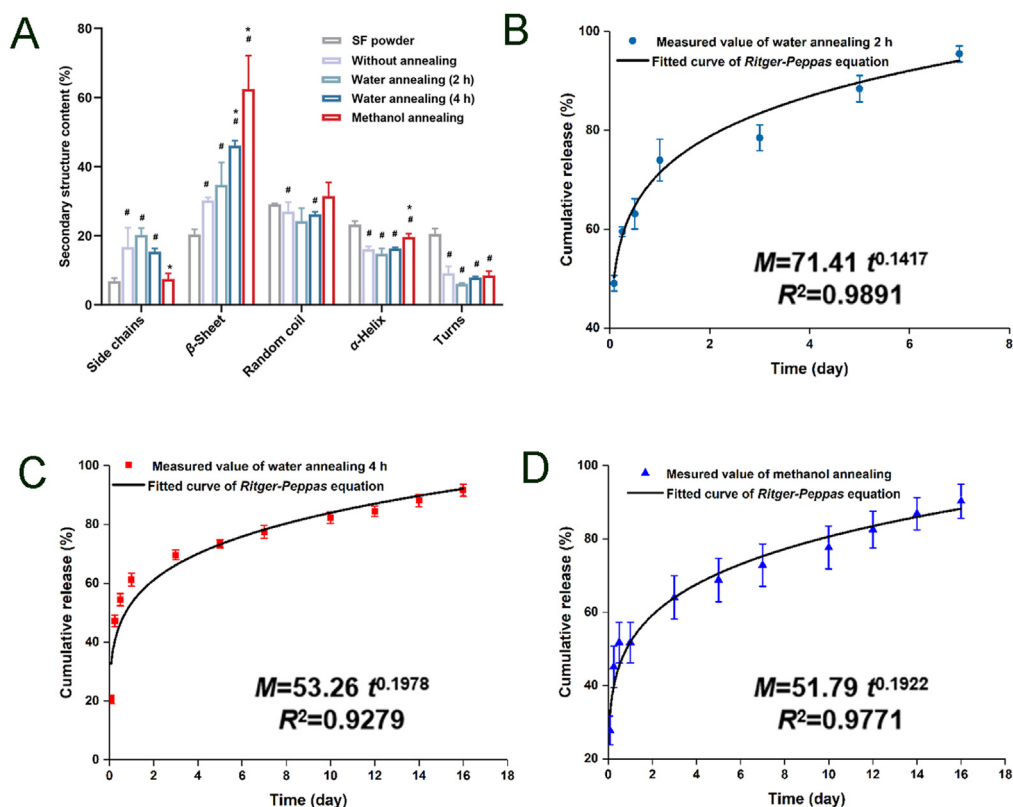


Figure 6 (A) Secondary structure content of MN patches with different annealing condition. Data are mean \pm SD, $n = 3$; $\#P < 0.05$ vs. SF powder; $*P < 0.05$ vs. Without annealing. (B–D) Equation fitting for release profiles of MN patch water annealing for 2 h, 4 h and methanol annealing for 0.5 h.

control group. After three consecutive weeks of treatment, the weight and height of the S.C. injection group was increased 54.78 ± 5.97 g and 6.76 ± 1.70 cm, respectively. There was no significant difference with the MN patch group which was 52.07 ± 5.94 g and 8.71 ± 2.74 cm, respectively (Fig. 9B and C). These results prove that in terms of increasing the weight and height of GHD mice, a weekly MN patch could achieve similar therapeutic effects as daily S.C. injection.

Adult patients with GHD can cause osteoporosis, increase the risk of fractures, and seriously affect the patient's quality of life. To access

whether the MN patch could improve the quality of the bone, the tibia slice of rats with different treatment were observed. Trabecular thickness (Tb. Th), trabecular number (Tb. N), trabecular separation (Tb. Sp) and the area of Tb are critical factors to evaluate the quality of the bone. As shown in Fig. 10A, Tb in normal control group was sturdy with complete structure and exhibited relatively small Tb. Sp, indicating the growing status of bone was well. Contrary, Tb in negative control group displayed relatively big Tb. Sp with twists and breaks and possessed less Tb. N, the area ratio of Tb was also small, all these results suggested poor quality of bone in GHD rats. rhGH-

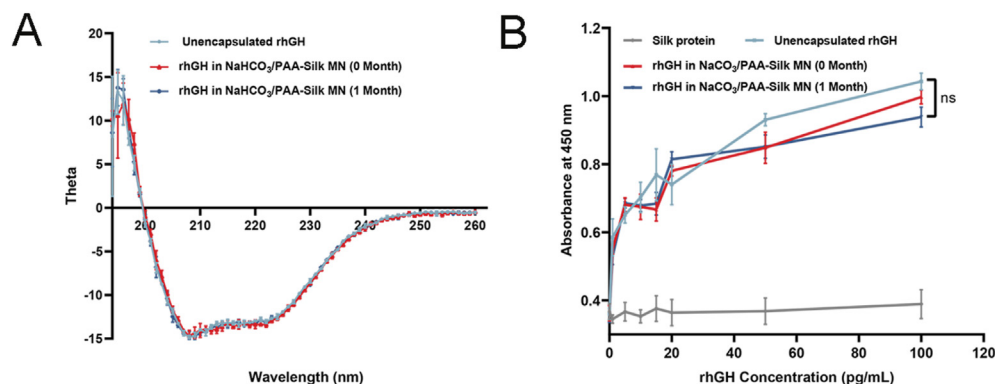


Figure 7 (A) Circular dichroism analysis of different extracted rhGH. Data are mean \pm SD, $n = 3$. (B) Cell proliferation assay of different extracted rhGH. Data are mean \pm SD, $n = 6$. ns, no significant.

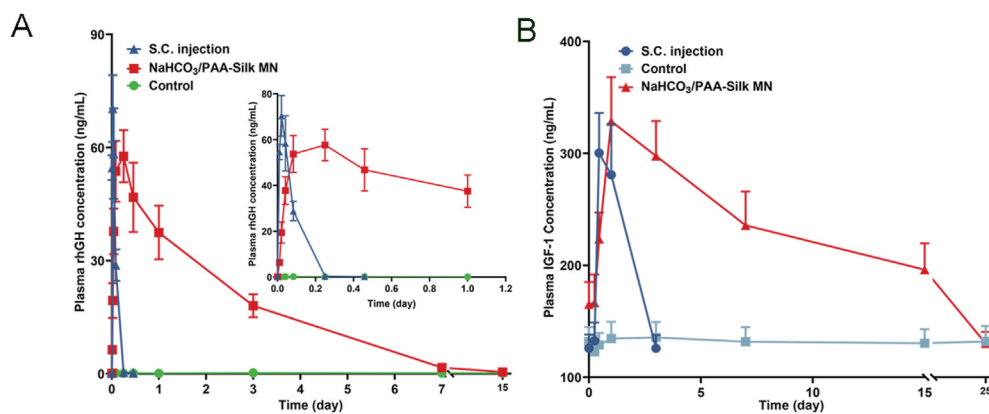


Figure 8 (A) Plasma rhGH levels in Sprague Dawley rat administration of NaHCO₃/PAA-Silk MN patch or S.C. injection of rhGH. (B) Plasma IGF-1 levels in Sprague Dawley rats administration of NaHCO₃/PAA-Silk MN patch or S.C. injection of rhGH. Data are mean \pm SD, $n = 5$.

treated groups significantly improved the area of Tb and induced Tb. Sp, the bone morphology and structure were relatively complete. The quantitative analysis of Tb in Fig. 10B–E were also shown the quality of the bone in the GHD rats was improved by rhGH-treated groups, and the MN patch exhibited similar treatments with S.C. injection group.

3.8. *In vivo* biodegradation and biocompatibility study

Although silk protein has been used in clinical applications for many years as a biodegradable material, the intradermal degradation behavior of silk protein-based MN system has not been reported. In order to explore the biodegradation behavior of PAA/NaHCO₃-Silk MN after it was applied to the skin, we constructed a “visualization and quantifiable” platform for PAA/NaHCO₃-Silk MN patch by TRITC-silk. PAA/NaHCO₃-Silk MN patch was applied to mice skin for 1 min, most of the MNs separated from the backing paper (Fig. 11A and B1), which was in reasonable agreement with the high detachment efficacy of the MN patch was applied to the porcine skin *ex vivo*. The fluorescence intensity of the MN patch inserted site gradually decreased over time and almost no fluorescence intensity could be detected after 21 days (Fig. 11B2–B8), demonstrating TRITC-silk was completely degraded *in vivo*. The degradation behavior of the MNs *in vivo* is different from that *in vitro*. *In vitro*, the silk protein transforms into a stable insoluble structure, remaining structurally intact of MNs during the release period with almost no erosion phenomenon. However, *in vitro* experiments were in the absence of cell-mediated biodegradation. *In vivo*, the MNs were slowly degraded and completely degraded in 21 days.

Interestingly, the degradation of the MN system prepared from silk protein in the intradermal is much faster than previously reported in the literature^{47,48}. However, it is worth noting that the total amount of silk protein was $\sim 540 \mu\text{g}$ per patch with diameter was less than 300 μm , silk protein and rhGH are evenly distributed in the MN system. Therefore the dissolved and diffused rhGH would form a porous structure of MNs and increase the surface area in contact with the tissue fluid. All these factors may cause the degradation of the silk protein MN to accelerate.

Biocompatibility is important for the development of a smart drug delivery systems. Based on previous studies, silk protein could be degraded into non-inflammatory amino acids *in vivo* and has good compatibility. For PAA/NaHCO₃-Silk MN, its administration method and depth are different from traditional

subcutaneous administration. Therefore the biocompatibility of the system needs to be proven. The results of the toxicity test of the components of the PAA/NaHCO₃-Silk MN patch on 3T3 cells showed that the components of the microneedles had good biological safety (Supporting Information Fig. S7). Examination of the rats during this study showed that PAA/NaHCO₃-Silk MN patches were well tolerated, with no erythema, edema, or other signs of irritation during the 21-day study. The MN before and after application to the skin was observed with a microscope displayed a high separation efficacy of MNs (Supporting Information Fig. S4A). Slight redness occurred at administration site, created micropores in the skin. The skin self-healed, the micropores disappeared, and the skin returned to normal after 2 h (Fig. S4B). The examination of the skin after treatment showed no obvious adverse effects (Fig. S4C). In short, the PAA/NaHCO₃-Silk MN system we constructed has superior biodegradability with completely degraded in 21 days. The smart system possesses good biocompatibility with no obvious side effects shown during 21-day treatment.

4. Discussion

Duo to most of GHD patients are not treated or have unsatisfactory treatment effects, the follow-up healthcare cost of these patients is high. Therefore, GHD has become a serious healthcare burden^{49,50}. Daily subcutaneous injection of rhGH brings severe pain to patients, while marketed LAGH is also inevitable subcutaneous injection and types and regions are limited. Low compliance of current treatment methods and extremely limited drug accessibility are the main obstacles of GHD treatment⁵¹. Therefore, there is an urgent need to develop a LAGH that better meet the need of the GHD patients.

To address these problems, we designed an active separation MN patch made from silk protein to sustained release of rhGH. The MN patch could realize self-management, complete

Table 1 Pharmacokinetic parameters of rhGH.

Parameter	S.C. injection group	NaHCO ₃ /PAA-Silk -rhGH MN
T_{max} (day)	0.03	0.26
C_{max} (ng/mL)	70.35 \pm 8.87	62.12 \pm 5.68
$t_{1/2}$ (day)	0.05	1.98
$\text{AUC}_{0-\infty}$ (ng·day/mL)	6.58 \pm 0.88	148.90 \pm 19.23

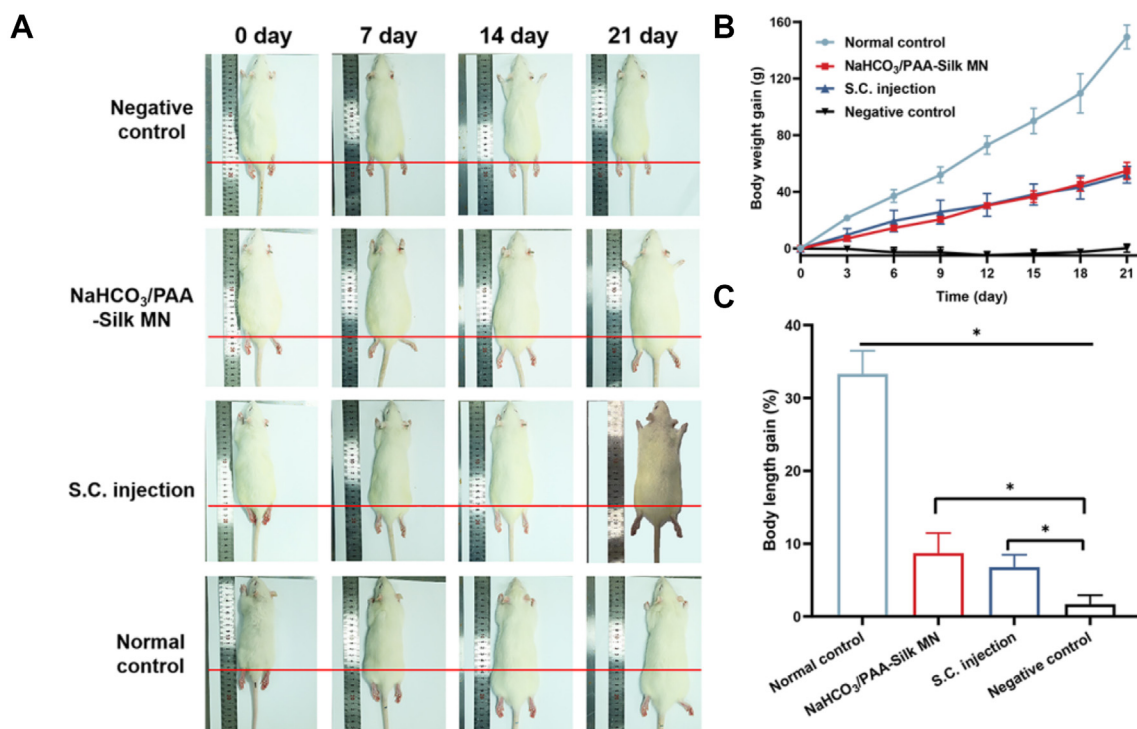


Figure 9 (A) Representative images of GHD rats after treated with NaHCO₃/PAA-Silk MN patch or S.C. injection of rhGH. (B) Body weight gained of GHD rats after treated with NaHCO₃/PAA-Silk MN patch or S.C. injection of rhGH in different time. (C) Body length gained of GHD rats after treated with NaHCO₃/PAA-Silk MN patch or S.C. injection of rhGH. Data are mean \pm SD, $n = 3$; * $P < 0.05$.

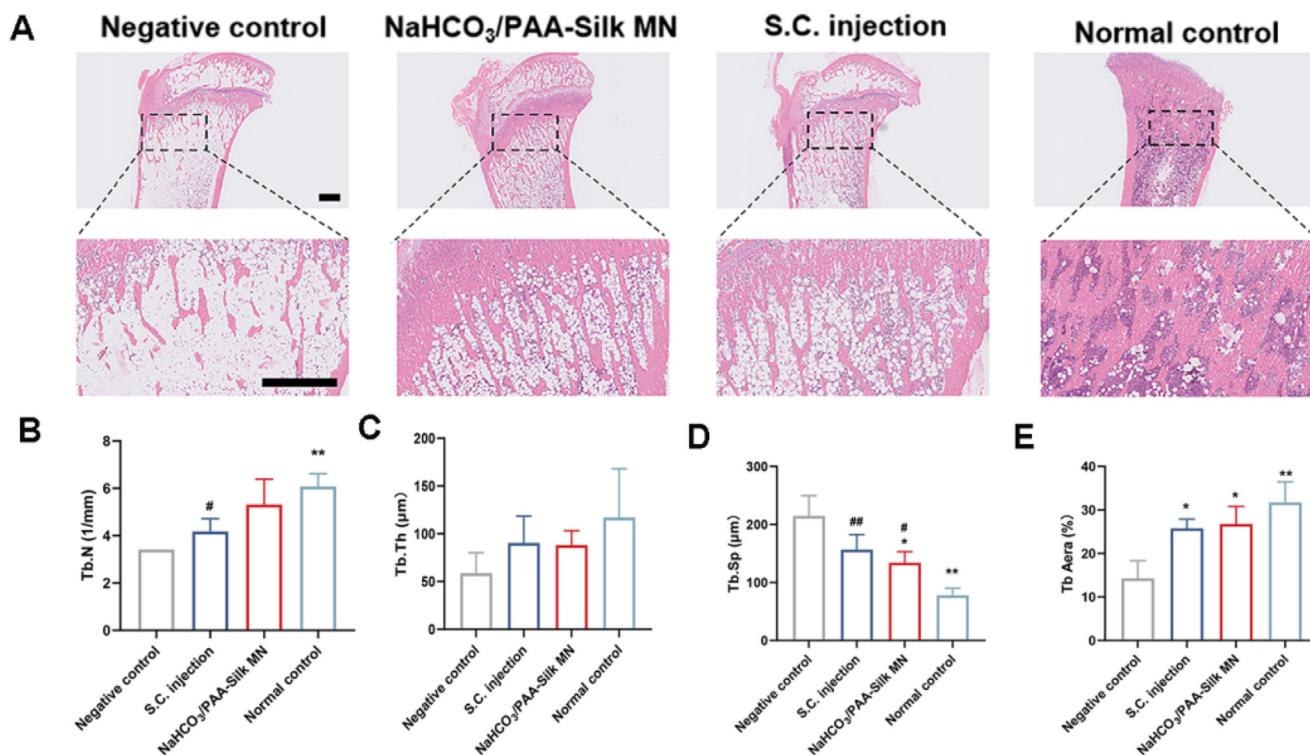


Figure 10 (A) Representative images of H&E staining after 21-day treatment with NaHCO₃/PAA-Silk MN patch or S.C. injection of rhGH. (B) Quantitative statistics of trabecular number (Tb.N). (C) Quantitative statistics of trabecular thickness (Tb.Th). (D) Quantitative statistics of trabecular thickness separation (Tb.Sp). (E) Quantitative statistics of area ratio of trabecular. Data are mean \pm SD, $n = 3$; * $P < 0.05$ vs. negative control; ** $P < 0.01$ vs. negative control; [#] $P < 0.05$ vs. normal control; ^{##} $P < 0.01$ vs. normal control. Scale bar = 1 mm.

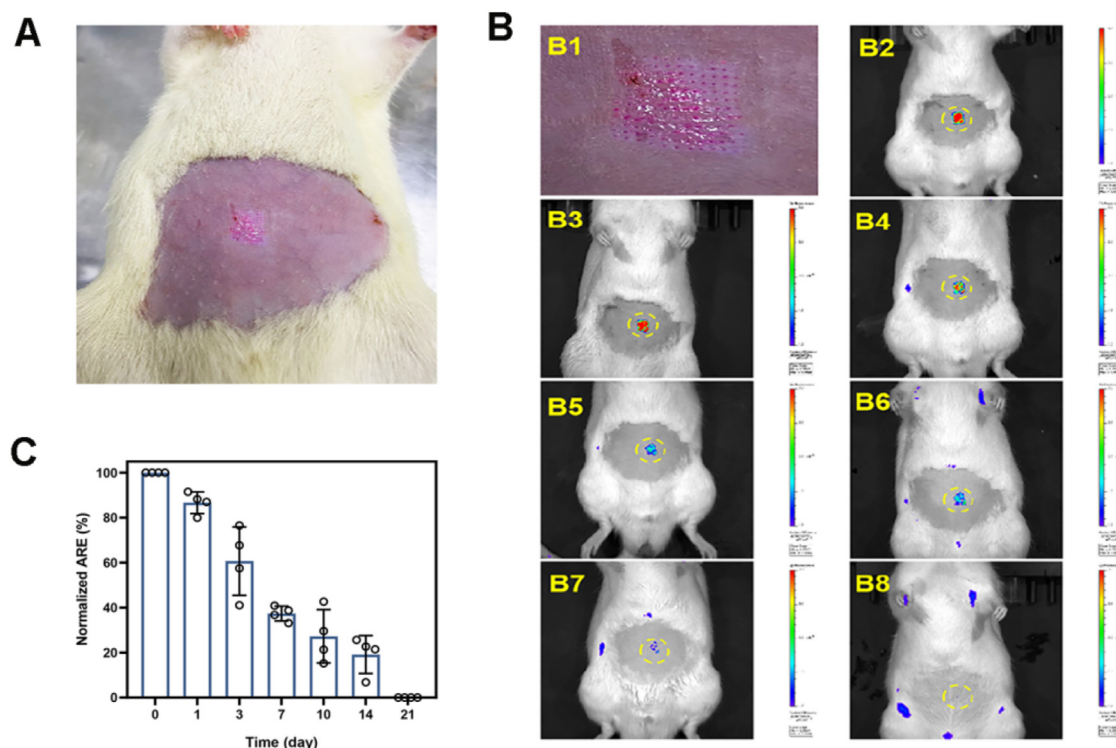


Figure 11 (A) Representative photograph of the rat abdomen after application of a $\text{NaHCO}_3/\text{PAA}$ -Silk MN patch made of TRITC-Silk. (B1) Representative magnified bright-field of A. (B2–B8) Representative fluorescence distribution in near-infrared *in vivo* imaging before and after (Days 0, 1, 3, 7, 10, 14 and 21) insertion of TRITC-Silk based MN patch into rat skin *in vivo*. The yellow circle represents the administration site of the MN patch. (C) Average radiant efficiency (ARE) of the skin after administration of TRITC-Silk based MN patch from Day 0–21. Data are deduced the ARE of skin of each rat before applied the MN patch. Data are mean \pm SD, $n = 4$.

administration within 1 min. After administration, no hazardous waste generated, and MNs implanted into the skin can achieve sustained release of rhGH for more than 7 days in rat. Moreover, the MN patch does not require cold chain transportation and storage, remains stable for 1 month at room temperature. We believe the MN patch for GHD treatment is safe and effective, because rhGH has been clinically used in the treatment of GHD for many years and has been proven to be safe and effective⁵². In addition, silk protein has a long history as surgical suture due to its superior biocompatibility, and MN patches (*albeit* not with separable MN patch) have been used successfully in clinical trials for bolus drug and vaccine delivery^{53–55}.

4.1. Rapid separation of the MN patch

In this study, effervescent substance NaHCO_3 was introduced into PAA separation layer of active separated MN patch to produce active backing. Upon the MN patch penetrating the skin and contact with ISF, the PAA was dissolved and generated H^+ , which reacted with HCO_3^{2-} immediately produced CO_2 gas bubbles that mechanically weakened the attachment of MNs to the backing paper and generates H_2O that facilitates dissolution of the MN-backing interface. These effects lead to the MNs detachment within 1 min after applied to the skin. Achieving rapid disintegration through effervescence is a classic method, often used in oral tablets⁵⁶. Mark R. Prausnitz et al.²⁹ developed a rapid MN patch by effervescence, which need to add additional citric acid to the prescription to produce H^+ , which may complicate the factors affecting the prescription. In this study, versatile PAA was used as both a soluble material

and an effervescent initiator to simplify the prescription. This rapid separation mediated by carrier material (PAA) and ISF requires no additional intervention by user and simplifies the application process. These advantages are necessary for the management of GHD patients, especially for pediatric patients. For pediatric patients with inherently active and poor self-control ability, rapid and simple dosing regimen will be more conducive to the self-management of children's families.

4.2. Sustained released of rhGH from the MN patch

Regulating the content of β -sheet in silk protein to control the release of therapeutics has been widely confirmed in previous studies^{57,58}. We have obtained MN patches with different β -sheet content through different processing conditions, which could control the release of rhGH from 1 day to over 16 days. All the patches shown burst release at 2 h, and the burst release decreased with the increase of β -sheet content, from 50% to 20%, similar results were found in work by Gong et al.⁵⁹. The burst release at 2 h may attribute to the uniform distribution of rhGH and silk protein, the rhGH embedded on the surface of the MN patch was released quickly. Actually, the burst release phenomenon also exists in other LAGH formulations. For example, LAGH made from PLGA developed by Jordan et al.³¹, the burst release of rhGH in 1 h was up to 33.9%–49.1%³¹. We believe that further increasing β -sheet content by increasing annealing time or change annealing media may reduce the burst release, which has been studied by Yavuz group³⁹, but no further research was done in this study. rhGH released from MN patch *in vitro* was dominated by

Fick diffusion, controlled release of rhGH over 16 days. However, *in vivo*, the diffusion of rhGH from the MN patch and degradable of silk MNs both play a role, hence rhGH released from MN patch *in vivo* was faster, the rhGH level in rat plasma was close to the normal value after 7 days. In the GHD mouse model, MN patch once a week can achieve similar therapeutic effects as daily S.C. injection, which means that the number of injection days per year treat with the MN patch could be reduced by up to 86%.

Our active separation MN patch contained rhGH $205.16 \pm 8.16 \mu\text{g}$ per patch shown $1.2 \text{ cm} \times 1.2 \text{ cm}$ (Fig. S6A), the dosage of a marketed daily hGH (Genotropin®) was 0.16–0.24 mg/kg/week for pediatric GHD. That means, a pediatric GHD with 30 kg need a $5.5 \text{ cm} \times 5.5 \text{ cm}$ patch for one week, which is close to the size of commercially available transdermal patches, such as EXELON® patch ($5\text{--}10 \text{ cm}^2$). However, additional work is required to verify the ease of administration of this size of MN patch. Unlike the current $1.2 \text{ cm} \times 1.2 \text{ cm}$ MN patch, accurate administration can be achieved easily by pressing with the thumb. In addition, increasing the concentration of rhGH during the manufacturing process or increasing the volume of the MNs can further enhance the drug loading, reducing the size of administration.

4.3. Increase access to LAGH and reduce costs

In the U.S., GHD-related costs were US \$18069–\$27893, of which 66%–86% was used to pay for somatotropin, a daily injection rhGH. To make matters worse, the health care-related costs of untreated GHD patients are twice that of treated GHD patients. These means that GHD has become a serious healthcare burden. Unfortunately, the types and regions of LAGH currently on the market are extremely limited, which leaves many GHD patients untreated.

In this study, we expected silk protein based rhGH MN patch could be transported and stored at room temperature, no need for professional healthcare personnel, which are important for countries and regions with scarce medical resources, increasing the availability of LAGH. Actually, many biologically active macromolecules have been demonstrated to maintain activity in silk protein membranes for a long time. For example, Vaxess Technologies (US) developed MN platform based on silk protein-MIMIX™ to deliver vaccine at room temperature. In our study, we demonstrated unmodified rhGH which loaded into silk protein MNs and exposed to a dry environment at room temperature for one month kept stable. Of course, longer time to investigate the stability of rhGH in silk protein MNs needs further study.

Secondly, the MN patch can implement self-management through simple training without obvious pain and does not require professional medical equipment assistance. Compared with marketed self-managed LAGH-Skytrofa, which was injected subcutaneous through an auto-injector, the MN patch was more conducive to the management of children with GHD. These advantages of the MN patch are extremely economical and can effectively reduce costs.

4.4. Study limitations and future work

There are some limitations in this study. For example, PK/PD studies of $\text{NaHCO}_3/\text{PAA-Silk}$ were only conducted in a relatively small number of SD rats. According to reports, the metabolism of rhGH in the rat model is faster than that of humans, so it is necessary to further verify the effect of the MN patch in primates. In addition, the drug loading of rhGH in $\text{NaHCO}_3/\text{PAA-Silk-rhGH}$

MN should be further increased, and the methods of increasing drug loading should be studied more comprehensively.

5. Conclusions

In this study, an actively separated MN patch made from silk protein was developed to treat GHD. An active layer was introduced into the MN patch, which enables MNs to separate from backing paper within 1 min after applied into the skin. The MN patch could release rhGH for >7 days *in vitro* and *in vivo* in rats. In GHD rat model, the MN patch administered once a week has the similar effects as daily S.C. injections. These results exhibited the potential of the MN patch as a LAGH. The structure and function of rhGH in the MN patch was preserved at least one month in a dry environment at room temperature, which demonstrated the MN patch as LAGH has the potential to avoid cold chain transportation and storage, possess great economic benefits. We speculate that actively separated MN patch could improve the treatment effect of GHD and provide a new self-management method for GHD patients.

Acknowledgments

We are grateful for the financial support from the National Natural Science Foundation of China (32071342 and 31922042), Guangdong Special Support Program (2019TQ05Y209), the Natural Science Foundation of Guangdong Province (2021A1515010431), the Fundamental Research Funds for the Central Universities (Nos. 2021-RC310-005, 2020-RC320-002 and 2019PT320028), and Chinese Academy of Medical Sciences Innovation Fund for Medical Sciences (2021-I2M-1-058).

Author contributions

Li Yang performed the majority of the experiments. Qingyun Liu and Xinhui Wang assisted in all animal experiments. Xiaowei Zeng, Lin Mei and Hongzhong Chen designed the overall project and supervised the whole work. Nansha Gao and Xiuzhen Li analyzed the data and wrote the manuscript with help from all authors.

Conflicts of interest

The authors declare no conflicts of interest.

Appendix A. Supporting information

Supporting data to this article can be found online at <https://doi.org/10.1016/j.apsb.2022.04.015>.

References

- Lin E, Wexler TL, Nachtigall L, Tritos N, Swearingen B, Hemphill L, et al. Effects of growth hormone deficiency on body composition and biomarkers of cardiovascular risk after definitive therapy for acromegaly. *Clin Endocrinol* 2012;**77**:430–8.
- Berryman DE, List EO. Growth hormone's effect on adipose tissue: quality versus quantity. *Int J Mol Sci* 2017;**18**:1621.
- Crespo I, Santos A, Webb SM. Quality of life in patients with hypopituitarism. *Curr Opin Endocrinol Diabetes Obes* 2015;**22**:306–12.
- Karachaliou F-H, Karavanaki K, Simatou A, Tsintzou E, Skarakis NS, Kanaka-Gatenbein C. Association of growth hormone deficiency (GHD) with anxiety and depression: experimental

- data and evidence from GHD children and adolescents. *Hormones* 2021;**20**:679–89.
5. Sievers C, Dimopoulou C, Pfister H, Lieb R, Steffin B, Roemmler J, et al. Prevalence of mental disorders in acromegaly: a cross-sectional study in 81 acromegalic patients. *Clin Endocrinol* 2009;**71**:691–701.
 6. Sprogoe K, Mortensen E, Karpf DB, Leff JA. The rationale and design of transcon growth hormone for the treatment of growth hormone deficiency. *Endocr Connect* 2017;**6**:R171–81.
 7. Fisher BG, Acerini CL. Understanding the growth hormone therapy adherence paradigm: a systematic review. *Horm Res Paediatr* 2013;**79**:189–96.
 8. Rosenfeld RG, Bakker B. Compliance and persistence in pediatric and adult patients receiving growth hormone therapy. *Endocr pract* 2008;**14**:143–54.
 9. Christiansen JS, Backeljauw PF, Bidlingmaier M, Biller BMK, Boguszewski MCS, Casanueva FF, et al. Growth hormone research society perspective on the development of long-acting growth hormone preparations. *Eur J Endocrinol* 2016;**174**:C1–8.
 10. Cutfield WS, Derraik JGB, Gunn AJ, Reid K, Delany T, Robinson E, et al. Non-compliance with growth hormone treatment in children is common and impairs linear growth. *PLoS One* 2011;**6**:e16223.
 11. Cawley P, Wilkinson I, Ross RJ. Developing long-acting growth hormone formulations. *Clin Endocrinol* 2013;**79**:305–9.
 12. Kaplowitz P, Manjelienskaia J, Lopez-Gonzalez L, Morrow CD, Pitukcheewanont P, Smith A. Economic burden of growth hormone deficiency in a US pediatric population. *J Manag Care Spec Pharm* 2021;**27**:1118–28.
 13. Diana JN, Tao Y, Du Q, Wang M, Kumar CU, Wu F, et al. PLGA microspheres of hGH of preserved native state prepared using a self-regulated process. *Pharmaceutics* 2020;**12**:683.
 14. Teva Pharmaceutical Industries Ltd. A phase 2, randomized, open-label, safety and dose-finding study comparing 3 different doses of weekly TV-1106 and daily recombinant human growth hormone (Genotropin) therapy in treatment-naïve, pre-pubertal, growth hormone-deficient children. Petach Tikva, Israel: Teva Pharmaceutical Industries Ltd.; 2016. EudraCT number 2013-004468-69, <https://www.clinicaltrialsregister.eu/ctr-search/trial/2013-004468-69/results>.
 15. Reiter EO, Attie KM, Moshang T, Silverman BL, Kemp SF, Neuwirth RB, et al. A multicenter study of the efficacy and safety of sustained release GH in the treatment of naïve pediatric patients with GH deficiency. *J Clin Endocrinol Metab* 2001;**86**:4700–6.
 16. Amereller F, Schilbach K, Schopohl J, Stoermann S. Adherence, attitudes and beliefs of growth hormone deficient patients—a questionnaire-based cohort study. *Exp Clin Endocrinol Diabetes* 2021;**129**:112–7.
 17. Goma Y, Kolluru C, Milewski M, Lee D, Zhang JT, Saklatvala R, et al. Development of a thermostable oxytocin microneedle patch. *J Contr Release* 2021;**337**:81–9.
 18. Courtenay AJ, McAlister E, McCrudden MTC, Vora L, Steiner L, Levin G, et al. Hydrogel-forming microneedle arrays as a therapeutic option for transdermal esketamine delivery. *J Contr Release* 2020;**322**:177–86.
 19. Du GS, He PH, Zhao JX, He CT, Jiang M, Zhang ZH, et al. Polymeric microneedle-mediated transdermal delivery of melittin for rheumatoid arthritis treatment. *J Contr Release* 2021;**336**:537–48.
 20. Xia DN, Jin R, Byagathvalli G, Yu H, Ye L, Lu CY, et al. An ultra-low-cost electroporator with microneedle electrodes (ePatch) for SARS-CoV-2 vaccination. *Proc Natl Acad Sci U S A* 2021;**118**:e2110817118.
 21. Kim YC, Lee JW, Esser ES, Kalluri H, Joyce JC, Compans RW, et al. Fabrication of microneedle patches with lyophilized influenza vaccine suspended in organic solvent. *Drug Deliv Transl Res* 2021;**11**:692–701.
 22. O'Shea J, Prausnitz MR, Roupael N. Dissolvable microneedle patches to enable increased access to vaccines against SARS-CoV-2 and future pandemic outbreaks. *Vaccines* 2021;**9**:320.
 23. Li GH, Badkar A, Nema S, Kolli CS, Banga AK. *In vitro* transdermal delivery of therapeutic antibodies using maltose microneedles. *Int J Pharm* 2009;**368**:109–15.
 24. Yu JC, Zhang YQ, Ye YQ, DiSanto R, Sun WJ, Ranson D, et al. Microneedle-array patches loaded with hypoxia-sensitive vesicles provide fast glucose-responsive insulin delivery. *Proc Natl Acad Sci U S A* 2015;**112**:8260–5.
 25. Chen MC, Lin ZW, Ling MH. Near-infrared light-activatable microneedle system for treating superficial tumors by combination of chemotherapy and photothermal therapy. *ACS Nano* 2016;**10**:93–101.
 26. Ye YQ, Yu JC, Wang C, Nguyen NY, Walker GM, Buse JB, et al. Microneedles integrated with pancreatic cells and synthetic glucose-signal amplifiers for smart insulin delivery. *Adv Mater* 2016;**28**:3115–21.
 27. Li W, Tang J, Terry RN, Li S, Brunie A, Callahan RL, et al. Long-acting reversible contraception by effervescent microneedle patch. *Sci Adv* 2019;**5**:eaaw8145.
 28. Lee Y, Li W, Tang J, Schwendeman SP, Prausnitz MR. Immediate detachment of microneedles by interfacial fracture for sustained delivery of a contraceptive hormone in the skin. *J Contr Release* 2021;**337**:676–85.
 29. Li W, Terry RN, Tang J, Feng MR, Schwendeman SP, Prausnitz MR. Rapidly separable microneedle patch for the sustained release of a contraceptive. *Nat Biom Eng* 2019;**3**:220–9.
 30. Tsiorkis K, Raja WK, Pritchard EM, Panilaitis B, Kaplan DL, Omenetto FG. Fabrication of silk microneedles for controlled-release drug delivery. *Adv Funct Mater* 2012;**22**:330–5.
 31. Jordan F, Naylor A, Kelly CA, Howdle SM, Lewis A, Illum L. Sustained release hGH microsphere formulation produced by a novel supercritical fluid technology: *in vivo* studies. *J Contr Release* 2010;**141**:153–60.
 32. Wang Y, Blasioli DJ, Kim H-J, Kim HS, Kaplan DL. Cartilage tissue engineering with silk scaffolds and human articular chondrocytes. *Biomaterials* 2006;**27**:4434–42.
 33. Jiang C, Wang X, Gunawidjaja R, Lin YH, Gupta MK, Kaplan DL, et al. Mechanical properties of robust ultrathin silk fibroin films. *Adv Funct Mater* 2007;**17**:2229–37.
 34. Stinson JA, Raja WK, Lee S, Kim HB, Diwan I, Tutunjian S, et al. Silk fibroin microneedles for transdermal vaccine delivery. *ACS Biomater Sci Eng* 2017;**3**:360–9.
 35. Jin HJ, Kaplan DL. Mechanism of silk processing in insects and spiders. *Nature* 2003;**424**:1057–61.
 36. Lu Q, Hu X, Wang XQ, Kluge JA, Lu SZ, Cebe P, et al. Water-insoluble silk films with silk I structure. *Acta Biomater* 2010;**6**:1380–7.
 37. Hu X, Shmelev K, Sun L, Gil ES, Park SH, Cebe P, et al. Regulation of silk material structure by temperature-controlled water vapor annealing. *Biomacromolecules* 2011;**12**:1686–96.
 38. Yavuz B, Chambre L, Harrington K, Kluge J, Valenti L, Kaplan DL. Silk fibroin microneedle patches for the sustained release of levonorgestrel. *ACS Appl Bio Mater* 2020;**3**:5375–82.
 39. Yavuz B, Morgan JL, Herrera C, Harrington K, Perez-Ramirez B, LiWang PJ, et al. Sustained release silk fibroin discs: antibody and protein delivery for HIV prevention. *J Contr Release* 2019;**301**:1–12.
 40. Hu XA, Wang XL, Rnjak J, Weiss AS, Kaplan DL. Biomaterials derived from silk-tropoelastin protein systems. *Biomaterials* 2010;**31**:8121–31.
 41. Park SH, Gil ES, Shi H, Kim HJ, Lee K, Kaplan DL. Relationships between degradability of silk scaffolds and osteogenesis. *Biomaterials* 2010;**31**:6162–72.
 42. Gong H, Wang J, Zhang J, Wu JB, Zheng ZZ, Xie XS, et al. Control of ocreotide release from silk fibroin microspheres. *Mater Sci Eng C Mater Biol Appl* 2019;**102**:820–8.
 43. Hu X, Kaplan D, Cebe P. Determining beta-sheet crystallinity in fibrous proteins by thermal analysis and infrared spectroscopy. *Macromolecules* 2006;**39**:6161–70.
 44. He S, Shi J, Walid E, Zhang H, Ma Y, Xue SJ. Reverse micellar extraction of lectin from black turtle bean (*Phaseolus vulgaris*): optimisation of extraction conditions by response surface methodology. *Food Chem* 2015;**166**:93–100.
 45. Gout PW, Beer CT, Noble RL. Prolactin-stimulated growth of cell cultures established from malignant Nb rat lymphomas. *Cancer Res* 1980;**40**:2433–6.

46. Park MR, Seo BB, Song SC. Dual ionic interaction system based on polyelectrolyte complex and ionic, injectable, and thermosensitive hydrogel for sustained release of human growth hormone. *Biomaterials* 2013;**34**:1327–36.
47. Greenwald D, Shumway S, Albear P, Gottlieb L. Mechanical comparison of 10 suture materials before and after *in vivo* incubation. *J Surg Res* 1994;**56**:372–7.
48. Bucknall TE, Teare L, Ellis H. The choice of a suture to close abdominal incisions. *Eur Surg Res* 1983;**15**:59–66.
49. Graham S, Auyeung V, Weinman J. Exploring potentially modifiable factors that influence treatment non-adherence amongst pediatric growth hormone deficiency: a qualitative study. *Patient Prefer Adherence* 2020;**14**:1889–99.
50. Hakkaart-van Roijen L, Beckers A, Stevenaert A, Rutten FF. The burden of illness of hypopituitary adults with growth hormone deficiency. *Pharmacoeconomics* 1998;**14**:395–403.
51. Strasburger CJ, Vanuga P, Payer J, Pfeifer M, Popovic V, Bajnok L, et al. MOD-4023, a long-acting carboxy-terminal peptide-modified human growth hormone: results of a Phase 2 study in growth hormone-deficient adults. *Eur J Endocrinol* 2017;**176**:283–94.
52. Aimaretti G, Fanciulli G, Bellone S, Maccario M, Arvat E, Delitala G, et al. Enhancement of the peripheral sensitivity to growth hormone in adults with GH deficiency. *Eur J Endocrinol* 2001;**145**:267–72.
53. Roupheal NG, Paine M, Mosley R, Henry S, McAllister DV, Kalluri H, et al. The safety, immunogenicity, and acceptability of inactivated influenza vaccine delivered by microneedle patch (TIV-MNP 2015): a randomised, partly blinded, placebo-controlled, phase 1 trial. *Lancet* 2017;**390**:649–58.
54. Daddona PE, Matriano JA, Mandema J, Maa Y-F. Parathyroid hormone (1-34)-coated microneedle patch system: clinical pharmacokinetics and pharmacodynamics for treatment of osteoporosis. *Pharm Res (N Y)* 2011;**28**:159–65.
55. Hirobe S, Azukizawa H, Hanafusa T, Matsuo K, Quan Y-S, Kamiyama F, et al. Clinical study and stability assessment of a novel transcutaneous influenza vaccination using a dissolving microneedle patch. *Biomaterials* 2015;**57**:50–8.
56. Liu F, Ranmal S, Batchelor HK, Orlu-Gul M, Ernest TB, Thomas IW, et al. Patient-centred pharmaceutical design to improve acceptability of medicines: similarities and differences in paediatric and geriatric populations. *Drugs* 2014;**74**:1871–89.
57. Boopathy AV, Mandal A, Kulp DW, Menis S, Bennett NR, Watkins HC, et al. Enhancing humoral immunity via sustained-release implantable microneedle patch vaccination. *Proc Natl Acad Sci U S A* 2019;**116**:16473–8.
58. DeMuth PC, Min Y, Irvine DJ, Hammond PT. Implantable silk composite microneedles for programmable vaccine release kinetics and enhanced immunogenicity in transcutaneous immunization. *Adv Healthc Mater* 2014;**3**:47–58.
59. Gong H, Wang J, Zhang J, Wu J, Zheng Z, Xie X, et al. Control of octreotide release from silk fibroin microspheres. *Mater Sci Eng C Mater Biol Appl* 2019;**102**:820–8.